Two representations in multifractal analysis

1995 J. Phys. A: Math. Gen. 28 5607

(http://iopscience.iop.org/0305-4470/28/19/015)

J. Phys. A: Math. Gen. 28 (1995) 5607–5622. Printed in the UK

Two representations in multifractal analysis

Jordi Mach†, Francesc Mas and Francesc Sagués

Departament de Química Física, Universitat de Barcelona C Martí Franquès 1, E-08028 Barcelona, Spain

Received 20 March 1995, in final form 9 June 1995

Abstract. Two representations in multifractal analysis, the so-called q and τ representations, are discussed theoretically and computed practically. Complementary to the standard q-representation, the so-called τ-representation is especially suited to resolving the most rarified subsets of the distributed measure. Moreover, these two representations are especially adapted, respectively, to the well known fixed-size and fixed-mass box-counting algorithms. Both strategies are first applied to iteratively constructed mathematical measures. Once tested in this way, we use them to analyse the mass distribution and the growth probability distribution of an experimental electrodeposited pattern.

1. Introduction

Currently the characterization of a measure distributed on a support may be attempted by using elements of multifractal analysis [1, 2]. Both the measure and the support are in practice obtained either from iterative mathematical processes or from experimental data. One way to base the multifractal analysis is proposed by Falconer [3] through the use of the expression

$$\Phi(q,\tau) = E\left(\sum_{i=1}^{N} p_i^q \varepsilon_i^{-\tau}\right) \tag{1}$$

where q and τ are real numbers and p_i and ε_i are random quantities that represent, respectively, the measure factor and the size factor. The sum is extended over all the separated parts, N, composing the object and E denotes expectation (the average value). Defined in this way, the function Φ represents the coupled q-moment of the measure and the $-\tau$-moment of the size‡. When exactly iterated mathematical measures are examined in this way the values q and τ are shown to satisfy $\Phi(q,\tau) = 1$ [7], and thus expression (1) can be written as

$$\sum_{i=1}^{N} p_i^q \varepsilon_i^{-\tau} = 1\,. \tag{2}$$

On the other hand, when an attempt is made to characterize an experimental measure, expression (1), resolved either with $p_i = cnt$ or $\varepsilon_i = cnt$, is assumed to collapse into a constant value function $\Phi(q,\tau)$.

† E-mail address: jordi@daphne.qf.ub.es

‡ In some more mathematically oriented papers [3, 4] a positive variable is defined as $\beta \equiv -\tau$, and in others [5, 6] they use $\gamma \equiv -\tau$.

0305-4470/95/195607+16$19.50

If $\varepsilon_i = cnt$, the size factor (ε) can be taken out of the sum. Then directly from (1),

$$\varepsilon \sim cnt \Rightarrow E\left\{\sum_{i=1}^{N(\varepsilon)} p_i^q\right\} \sim \varepsilon^{\tau} \tag{3}$$

where $N(\varepsilon)$ is the number of parts with size ε, needed to cover the whole support where the measure is defined.

On the other hand, if the averaged quantity in (1) is weighted with the probability distribution p_i, we have

$$\langle p^{(q-1)}\varepsilon^{-\tau}\rangle_p \sim cnt\,. \tag{4}$$

Now, if we take $p = cnt$, expression (4) converts into

$$p \sim cnt \Rightarrow \langle \varepsilon^{-\tau}\rangle_p \sim p^{1-q} \tag{5}$$

where $\langle\,\rangle_p$ indicates the average value computed according to the probability distribution p_i.

In this way we have derived two alternative representations of multifractal indices, taking either q or τ as the fundamental moment. Note, in addition, that according to their respective definitions, each one of these representations is particularly well adapted to one of the two versions of the box-counting algorithms, i.e. fixed-size or fixed-mass [5, 6, 8, 9], commonly used in this context.

The multifractal indices used to characterize a non-uniform measure are: (i) the set of generalized fractal dimensions $D_q = \tau/(q-1)$ introduced by Grassberger, Hentschel and Procaccia [8–10]; (ii) the so-called Hölder exponent [1] α, satisfying $\alpha = \mathrm{d}\tau/\mathrm{d}q$; and (iii) the Legendre transformed function $f(\alpha)$, defined as $f(\alpha) = q\alpha - \tau$. The primary aim of this paper is then to conveniently express and interpret these multifractal indices in the two representations commented on above.

In section 2 we review the well known properties of the functions α and $f(\alpha)$ expressed in terms of q. Hereafter, we refer to this formulation as the q-representation. Alternatively, in section 3 we present the properties of the functions α and $f(\alpha)$ expressed in terms of τ. Hereafter, we refer to this formulation as the τ-representation. In order to show the complementary nature of these two representations, in section 4, we present three examples generated via an iterated mathematical process [7, 11], for which the multifractal behaviour may be solved exactly: one generated with the size factor fixed, the other generated with the measure factor fixed and the third one generated without fixing any of the factors which define the measure. In section 5 we show how this dual formalism is easily adapted to box-counting algorithms in their versions of fixed size or fixed mass. These algorithms are first tested with the mathematical generated examples of multifractal measures introduced in section 4. Finally, in section 6 we apply these algorithms to two measures (mass distribution and growth probability distribution, GPD) defined on an experimental electrodeposited pattern.

2. Properties of the multifractal indices in the q-representation

Here we summarize the most important properties of the multifractal indices in the q-representation (3) (demonstrations can be found in Halsey *et al* [7] and in Cawley and Mauldin [4]). In this case $\tau = \tau(q)$. Moreover, $\tau'(q) = \mathrm{d}\tau(q)/\mathrm{d}q = \alpha(q) \equiv \alpha_q \equiv \alpha$ and the Legendre transform of $\tau(q)$ is $f(\alpha(q)) = q\alpha(q) - \tau(q) \equiv f(\alpha) \equiv f_q \equiv f$. From the fact that $\tau'(q) > 0$, $\tau(q)$ is a strictly increasing function of q, $\tau_0 = -D_f$ (the fractal

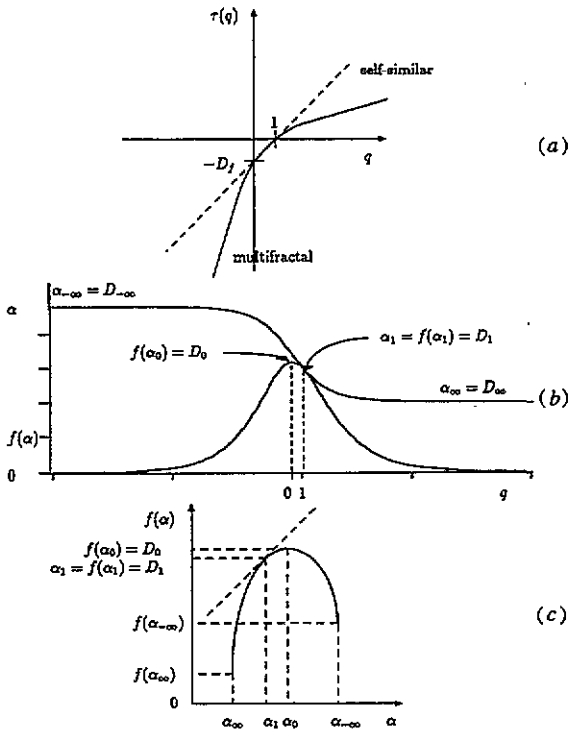

Figure 1. Multifractal indices in the q-representation. (a) Plot of $\tau(q)$ versus q. (b) Plot of $\alpha(q)$ and $f(\alpha(q))$ versus q. (c) Spectrum of singularities $f(\alpha)$.

Table 1. Properties of the multifractal indices in the q-representation.

q	Characteristic values
$-\infty$	$D_{-\infty} = \alpha_{-\infty} = \alpha_{max} > 0$ $D_f \geqslant f(\alpha_{-\infty}) \geqslant 0$
0	$D_0 = D_f$ $\tau_0 = -D_f$ $f(\alpha_0) = f_{max} = D_f$
1	$\tau_1 = 0$ $D_1 = \alpha_1 = f(\alpha_1)$
$+\infty$	$D_{+\infty} = \alpha_{+\infty} = \alpha_{min} > 0$ $D_f \geqslant f(\alpha_{+\infty}) \geqslant 0$

dimension of the support of the measure, which coincides with D_0) and $\tau_1 = 0$. In [4] it is demonstrated that either $\tau''(q) < 0$ or $\tau''(q) = 0$, which, respectively, implies that $\alpha(q)$ is either strictly decreasing (multifractal measure) or constant and equal to D_f (self-similar measure). It is easy to see from the Legendre transform that $f_0 = D_f$, $f_1 = \alpha_1 = D_1$ and $f'(\alpha(q)) = q\tau''(q)$. So either $f(\alpha)$ is constantly equal to D_f or $f(\alpha)$ is strictly increasing from $q = -\infty$ to $q = 0$ and strictly decreasing from $q = 0$ to ∞. The asymptotic behaviour of $\alpha(q)$ and $f(\alpha(q))$ when $q \to \pm\infty$ can be summarized in the following way: $\alpha_{\pm\infty} = D_{\pm\infty}$ is a finite positive number and $D_f \geqslant f(\alpha_{\pm\infty}) \geqslant 0$. All these properties are summarized in figure 1 and table 1.

3. Properties of the multifractal indices in the τ-representation

In this case we have, alternatively, $q = q(\tau)$. According to (5), the properties of the multifractal indices are, however, similar to those in the q-representation, with $-\tau$ playing the role of q and $1 - q(\tau)$ that of $\tau(q)$. We can thus define, as in [5, 6, 12], $\tilde{D}(\tau) = \tau/(q(\tau) - 1) \equiv \tilde{D}_\tau$. Moreover, $\mathrm{d}(1 - q(\tau))/\mathrm{d}(-\tau) = \mathrm{d}q(\tau)/\mathrm{d}\tau = q'(\tau) \equiv \tilde{\alpha}(\tau) \equiv \tilde{\alpha}_\tau \equiv \tilde{\alpha}$, which implies that $\tilde{\alpha}$ and $-\tau$ are conjugated variables. Then, the Legendre transform of $(1 - q(\tau))$ is $\tilde{f}(\tilde{\alpha}(\tau)) = -\tau\tilde{\alpha}(\tau) - (1 - q(\tau)) \equiv \tilde{f}(\tilde{\alpha}) \equiv \tilde{f}_\tau \equiv \tilde{f}$. It is easy to demonstrate that $q'(\tau) > 0$ and then that $q(\tau)$ is a strictly increasing function of τ, $q_0 = 1$

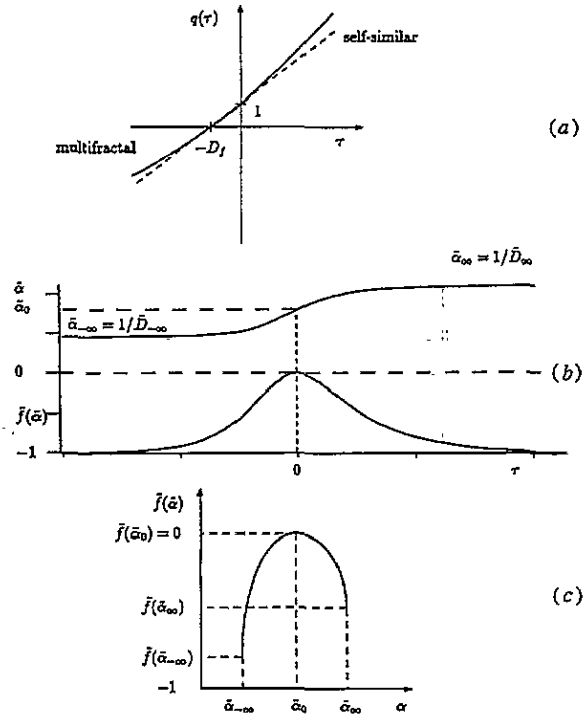

Figure 2. Multifractal indices in the τ-representation. (*a*) Plot of $q(\tau)$ versus τ. (*b*) Plot of $\tilde{\alpha}$ and $\tilde{f}(\tilde{\alpha})$ versus τ. (*c*) Spectrum of singularities $\tilde{f}(\tilde{\alpha})$.

Table 2. Properties of the multifractal indices in the τ-representation.

τ	Characteristic values
$-\infty$	$\tilde{\alpha}_{-\infty} = \tilde{\alpha}_{min} = 1/\tilde{D}_{-\infty} > 0$ $\tilde{D}_{-\infty} = D_{-\infty}$ $0 \geqslant \tilde{f}(\tilde{\alpha}_{-\infty}) \geqslant -1$
$-D_f$	$q_{-D_f} = 0$ $\tilde{D}_{-D_f} = D_f$
0	$q_0 = 1$ $\tilde{D}_0 = 1/\tilde{\alpha}_0$ $\tilde{f}(\tilde{\alpha}_0) = \tilde{f}_{max} = 0$
$+\infty$	$\tilde{\alpha}_{+\infty} = \tilde{\alpha}_{max} = 1/\tilde{D}_{+\infty} > 0$ $\tilde{D}_{+\infty} = D_{+\infty}$ $0 \geqslant \tilde{f}(\tilde{\alpha}_{+\infty}) \geqslant -1$

Table 3. Equivalences between the two representations.

Representation	q	τ
Moment	q	$-\tau$ [a]
Scaling exponent	$\tau(q)$	$1-q(\tau)$
Generalized dimensions	D_q	$\tilde{D}_\tau$ [b]
conjugate variable of the moment	$\alpha(q) = 1/\tilde{\alpha}(\tau)$	
Legendre transform of the scaling exponent	$f(\alpha(q)) = (1 + \tilde{f}(\tilde{\alpha}(\tau)))/\tilde{\alpha}(\tau)$ [c]	

[a] In [3, 4] $\beta = -\tau$ and in [5, 6] $\gamma = -\tau$.
[b] In [3, 12] $D_\gamma = \tilde{D}_\tau$.
[c] In [12] $\tilde{f}(\tilde{\alpha}(\tau)) = f(\alpha(q))/\alpha(q) - 1$.

and $q_{-Df} = 0$. Moreover, either $q''(\tau) > 0$ for all τ, or $q''(\tau) = 0$ which, respectively, implies that $\tilde{\alpha}(\tau)$ is either strictly increasing (multifractal measure) or constant and equal to $1/D_f$ (self-similar measure). It is easy to see from the Legendre transform that $\tilde{f}_0 = 0$ and $\tilde{f}'(\tilde{\alpha}(\tau)) = -\tau q''(\tau)$. Thus, either $\tilde{f}(\tilde{\alpha}(\tau))$ is constantly equal to 0 or $\tilde{f}(\tilde{\alpha}(\tau))$ is strictly increasing from $\tau = -\infty$ to $\tau = 0$ and strictly decreasing from $\tau = 0$ to $\tau = \infty$. The asymptotic behaviour of $\tilde{\alpha}(\tau)$ and $\tilde{f}(\tilde{\alpha}(\tau))$ for $\tau \to \pm\infty$ can be summarized in the following way: $\tilde{\alpha}_{\pm\infty}$ is a finite positive number and $0 > \tilde{f}(\tilde{\alpha}_{\pm\infty}) \geqslant -1$. All these properties are summarized in figure 2 and table 2. Furthermore, a summary of the equivalences between the two representations is presented in table 3.

4. Exactly soluble examples

Next we apply the previous formalisms to iterated mathematical measures. We start with an original region whose measure and size are taken arbitrarily as unity. Divide the region into N pieces with measure p_i and size ε_i. At the next step each piece of the set is further divided into N pieces, each with a measure reduced by a factor p_j and size reduced by a factor ε_j, and so on [7, 10, 11]. Figure 3 shows an example of this iterative method that allow us to construct multifractal measures with different size and different measure factors.

4.1. Example 1

If all pieces have the same size $\varepsilon_i = \varepsilon$, then from (2) [7, 11]

$$\tau = \frac{\log \sum_{i=1}^{N} p_i^q}{\log \varepsilon} \tag{6}$$

and since τ is expressed as a function of q, α and f admit simple expressions in this representation. Using the definitions quoted above we obtain

$$\alpha(q) = \frac{\sum_{i=1}^{N} \hat{p}_i \log p_i}{\log \varepsilon} \qquad f(q) = \frac{\sum_{i=1}^{N} \hat{p}_i \log \hat{p}_i}{\log \varepsilon} \tag{7}$$

where $\hat{p}_i = p_i^q / \sum_{j=1}^{N} p_j^q$.

The summarized results for the particular case of $N = 3$, $p_1 = \frac{3}{16}$, $p_2 = \frac{5}{16}$, $p_3 = \frac{8}{16}$ and $\varepsilon = \frac{1}{2}$ can be found in the first column of table 4.

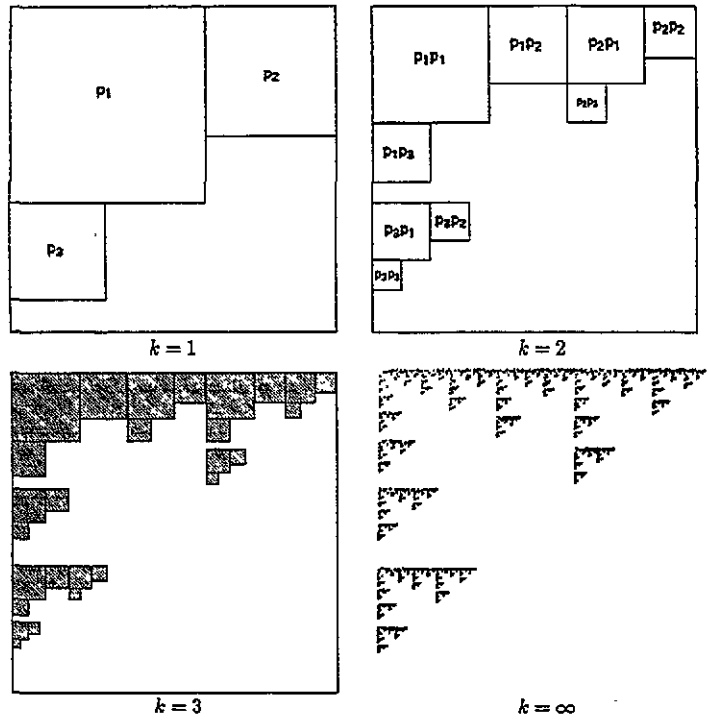

Figure 3. Example of the generation of an iterated mathematical multifractal with different size and different measure factors. Here we show the three first iterations and the infinite one.

Table 4. Some representative multifractal indices in the q-representation of the exactly soluble multifractal with equal size and different measure. The parameters are $N = 3$, $p_1 = \frac{3}{16}$, $p_2 = \frac{5}{16}$, $p_3 = \frac{8}{16}$ and $\varepsilon = \frac{1}{2}$. Computed results are obtained using a box-counting fixed-size algorithm on a grid of 512×512 pixels (scaling corresponds to $2.53 \leqslant \ell \leqslant 47.18$ pixels).

q	Singularity exponent	Mathematical result	Computed result
$-\infty$	$\alpha_{-\infty} = D_{-\infty}$	2.415 04	—
	$f(\alpha_{-\infty})$	0.000 00	—
-2	τ_{-2}	$-5.415\,64$	-5.2 ± 0.3
	D_{-2}	1.805 21	1.7 ± 0.3
	α_{-2}	2.105 63	3.7 ± 0.2
	$f(\alpha_{-2})$	1.204 37	0.2 ± 0.1
0	$f(\alpha_0) = D_0 = D_f$	1.589 46	1.61 ± 0.02
	α_0	1.697 70	1.72 ± 0.04
1	$f(\alpha_1) = \alpha_1 = D_1$	1.477 22	1.49 ± 0.01
3	$\tau_3 = 2D_3$	2.624 96	2.66 ± 0.04
20	τ_{20}	19.999 9	23.1 ± 0.2
	D_{20}	1.052 63	1.2 ± 0.2
	α_{20}	1.000 06	1.1 ± 0.1
	$f(\alpha_{20})$	0.001 24	0.2 ± 0.1
$+\infty$	$\alpha_{+\infty} = D_{+\infty}$	1.000 00	—
	$f(\alpha_{+\infty})$	0.000 00	—

4.2. Example 2

Another example is given by the case in which all pieces have equal measures, $p_i = p$, but different sizes, ε_i. In this case, manipulating (2) we obtain

$$q = -\frac{\log \sum_{i=1}^{N} \varepsilon_i^{-\tau}}{\log p} \tag{8}$$

and here q is clearly a function of τ, which allows us to use the τ-representation to obtain $\tilde{\alpha}$ and $\tilde{f}$. Note that (8) does not contain $(1 - q)$ because we need to start from (2) (iterative multifractal process) and not from (5) (experimental or simulated pattern). Using the definitions of $\tilde{\alpha}(\tau)$ and $\tilde{f}(\tilde{\alpha}(\tau))$ quoted above, we obtain

$$\tilde{\alpha}(\tau) = \frac{\sum_{i=1}^{N} \hat{\varepsilon}_i \log \varepsilon_i}{\log p} \qquad \tilde{f}(\tilde{\alpha}(\tau)) = \frac{\sum_{i=1}^{N} \hat{\varepsilon}_i \log \hat{\varepsilon}_i}{\log p} - 1 \tag{9}$$

where $\hat{\varepsilon}_i = \varepsilon_i^{-\tau} / \sum_{j=1}^{N} \varepsilon_j^{-\tau}$.

The first column of table 5 summarizes the multifractal behaviour in the τ-representation for the particular case of $N = 3$, $\varepsilon_1 = 0.6$, $\varepsilon_2 = 0.4$, $\varepsilon_3 = 0.3$ and $p = \frac{1}{3}$.

Table 5. Some representative multifractal indices in the τ-representation of the exactly soluble multifractal with equal measure and different size. The parameters are $N = 3$, $\varepsilon_1 = 0.6$, $\varepsilon_2 = 0.4$, $\varepsilon_3 = 0.3$ and $p = \frac{1}{3}$. Computed results are obtained using a box-counting fixed-mass algorithm on a grid of 512×512 pixels. The regression range is the standard in our fixed-mass algorithm.

τ	*Singularity exponent*	*Mathematical result*	*Computed result*
$-\infty$	$q_{-\infty}$	$-\infty$	—
	$\tilde{\alpha}_{-\infty}$	0.464 97	—
	$\tilde{f}(\tilde{\alpha}_{-\infty})$	−1.000 00	—
	$\tilde{D}_{-\infty}$	2.150 66	—
−50	q_{-50}	−23.249	-23.7 ± 0.2
	$\tilde{\alpha}_{-50}$	0.464 97	0.49 ± 0.01
	$\tilde{f}(\tilde{\alpha}_{-50})$	−1.000 00	-0.25 ± 0.06
	$\tilde{D}_{-50}$	2.061 97	2.03 ± 0.02
$-D_f$	q_{-D_f}	0.000 00	0.10 ± 0.01
	$\tilde{\alpha}_{-D_f}$	0.699 93	0.634 ± 0.005
	$\tilde{f}(\tilde{\alpha}_{-D_f})$	−0.065 30	-0.05 ± 0.01
	$\tilde{D}_{-D_f}$	1.335 43	1.49 ± 0.01
0	q_0	1.000 00	—
	$\tilde{\alpha}_0$	0.798 31	0.71 ± 0.01
	$\tilde{f}(\tilde{\alpha}_0)$	0.000 00	—
	$\tilde{D}_0$	1.252 65	1.41 ± 0.02
8	q_8	8.857 30	8.34 ± 0.07
	$\tilde{\alpha}_8$	1.069 93	1.01 ± 0.01
	$\tilde{f}(\tilde{\alpha}_8)$	−0.702 10	-0.77 ± 0.03
	$\tilde{D}_8$	1.018 16	1.09 ± 0.01
∞	q_∞	∞	—
	$\tilde{\alpha}_\infty$	1.095 90	—
	$\tilde{f}(\tilde{\alpha}_\infty)$	−1.000 00	—
	$\tilde{D}_\infty$	0.912 49	—

4.3. Example 3

In this last example we composed an object with neither the size nor the measure fixed (figure 3). In this case it is not possible to find an explicit function $q(\tau)$ or $\tau(q)$ from (2). In order to obtain the pair of values (q, τ), we use the Newton–Raphson method, which converges very quickly. For each pair of values (q, τ) the quantities $\alpha(q)$, $f(\alpha(q))$, $\tilde{\alpha}(\tau)$, $\tilde{f}(\tilde{\alpha}(\tau))$ are determined using the definitions explained in sections 2 and 3. The explicit expressions for $\alpha(q)$ and $f(\alpha(q))$ can be found in Cawley and Mauldin [4]:

$$\alpha(q) = \sum_{i=1}^{N} p_i^q \varepsilon_i^{-\tau} \log p_i \Big/ \sum_{i=1}^{N} p_i^q \varepsilon_i^{-\tau} \log \varepsilon_i \tag{10}$$

$$f(\alpha(q)) = \sum_{i=1}^{N} p_i^q \varepsilon_i^{-\tau} \log \left(p_i^q \varepsilon_i^{-\tau}\right) \Big/ \sum_{i=1}^{N} p_i^q \varepsilon_i^{-\tau} \log \varepsilon_i \,. \tag{11}$$

For the expressions of $\tilde{\alpha}(\tau)$ and $\tilde{f}(\tilde{\alpha}(\tau))$ we use the definitions introduced in section 3, which can be written as

$$\tilde{\alpha}(\tau) = \sum_{i=1}^{N} p_i^q \varepsilon_i^{-\tau} \log \varepsilon_i \Big/ \sum_{i=1}^{N} p_i^q \varepsilon_i^{-\tau} \log p_i \tag{12}$$

$$\tilde{f}(\tilde{\alpha}(\tau)) = \sum_{i=1}^{N} p_i^q \varepsilon_i^{-\tau} \log \left(p_i^{(q-1)} \varepsilon_i^{-\tau}\right) \Big/ \sum_{i=1}^{N} p_i^q \varepsilon_i^{-\tau} \log p_i \,. \tag{13}$$

The first columns of tables 6 and 7 summarize, respectively, the multifractal behaviour for the particular case $N = 3$, $\varepsilon_1 = 0.6$, $\varepsilon_2 = 0.4$, $\varepsilon_3 = 0.3$ and $p_1 = \frac{3}{16}$, $p_2 = \frac{5}{16}$, $p_3 = \frac{8}{16}$ when the q-representation and τ-representation are used. Note that in this case

Table 6. Some representative multifractal indices in the q-representation of the exactly soluble multifractal with different size and different measure. The parameters are $N = 3$, $\varepsilon_1 = 0.6$, $\varepsilon_2 = 0.4$, $\varepsilon_3 = 0.3$ and $p_1 = \frac{3}{16}$, $p_2 = \frac{5}{16}$, $p_3 = \frac{8}{16}$. Computed results are obtained using a box-counting fixed-size algorithm on a grid of 512×512 pixels (scaling corresponds to $3.43 \leqslant \ell \leqslant 109.7$ pixels).

q	Singularity exponent	Mathematical result	Computed result
$-\infty$	$\alpha_{-\infty} = D_{-\infty}$	3.277 00	—
	$f(\alpha_{-\infty})$	0.000 00	—
-2	τ_{-2}	−6.604 59	-4.2 ± 0.3
	D_{-2}	2.201 53	1.4 ± 0.3
	α_{-2}	3.183 21	3.1 ± 0.1
	$f(\alpha_{-2})$	0.238 16	0.4 ± 0.1
0	$f(\alpha_0) = D_0 = D_f$	1.335 43	1.37 ± 0.02
	α_0	1.726 03	1.73 ± 0.05
1	$f(\alpha_1) = \alpha_1 = D_1$	1.040 46	1.07 ± 0.03
3	$\tau_3 = 2D_3$	1.595 52	1.66 ± 0.07
20	τ_{20}	11.5143	12.1 ± 0.2
	D_{20}	0.606 02	0.6 ± 0.2
	α_{20}	0.575 72	0.61 ± 0.06
	$f(\alpha_{20})$	0.000 03	0.02 ± 0.05
$+\infty$	$\alpha_{+\infty} = D_{+\infty}$	0.575 72	—
	$f(\alpha_{+\infty})$	0.000 00	—

Table 7. Some representative multifractal indices in the τ-representation of the exactly soluble multifractal with different size and different measure. The parameters are $N = 3$, $\varepsilon_1 = 0.6$, $\varepsilon_2 = 0.4$, $\varepsilon_3 = 0.3$ and $p_1 = \frac{3}{16}$, $p_2 = \frac{5}{16}$, $p_3 = \frac{8}{16}$. Computed results are obtained using a box-counting fixed-mass algorithm on a grid of 512×512 pixels. The regression range is the standard in our fixed-mass algorithm.

τ	Singularity exponent	Mathematical result	Computed result
$-\infty$	$q_{-\infty}$	$-\infty$	—
	$\tilde{\alpha}_{-\infty}$	0.305 16	—
	$\tilde{f}(\tilde{\alpha}_{-\infty})$	−1.000 00	—
	$\tilde{D}_{-\infty}$	3.277 00	—
−50	q_{-50}	−15.258	-15.1 ± 0.7
	$\tilde{\alpha}_{-50}$	0.305 16	0.31 ± 0.01
	$\tilde{f}(\tilde{\alpha}_{-50})$	−1.000 00	-0.6 ± 0.3
	$\tilde{D}_{-50}$	3.075 44	3.1 ± 0.1
$-D_f$	q_{-D_f}	0.000 00	0.02 ± 0.03
	$\tilde{\alpha}_{-D_f}$	0.579 36	0.60 ± 0.02
	$\tilde{f}(\tilde{\alpha}_{-D_f})$	−0.226 40	-0.17 ± 0.01
	$\tilde{D}_{-D_f}$	1.335 43	1.37 ± 0.04
0	q_0	1.000 00	—
	$\tilde{\alpha}_0$	0.961 11	0.94 ± 0.01
	$\tilde{f}(\tilde{\alpha}_0)$	0.000 00	—
	$\tilde{D}_0$	1.040 46	1.12 ± 0.02
8	q_8	13.8959	12.7 ± 0.3
	$\tilde{\alpha}_8$	1.736 73	1.60 ± 0.04
	$\tilde{f}(\tilde{\alpha}_8)$	−0.997 93	-1.2 ± 0.2
	$\tilde{D}_8$	0.620 35	0.69 ± 0.02
∞	q_∞	∞	—
	$\tilde{\alpha}_\infty$	1.736 97	—
	$\tilde{f}(\tilde{\alpha}_\infty)$	−1.000 00	—
	$\tilde{D}_\infty$	0.575 72	—

the two representations may be equally used to characterize the multifractal behaviour of this distributed measure. It is also easy to check the equivalences between the two representations as listed in table 3.

5. Application to box-counting algorithms

When experimental, rather than mathematical, measures have to be examined in terms of their multifractal properties we need to resort to box-counting algorithms. The two most popular routines are the fixed-size and fixed-mass algorithms. As is shown in what follows, each one is particularly adapted to one of the two representations presented above.

5.1. Box-counting fixed-size algorithm

The well known fixed-size box-counting algorithm is based on (3) and the mean value is obtained as an averaged value of the so-called partition function $Z_q(\varepsilon) \equiv \sum_{i=1}^{N(\varepsilon)} p_i^q(\varepsilon)$ [8, 9]

$$\tau(q) = \lim_{\varepsilon \to 0} \frac{\log E\left(Z_q(\varepsilon)\right)}{\log \varepsilon}. \tag{14}$$

Clearly, in this case τ is expressed as a function of q. Thus it seems natural to use the q-representation to obtain expressions for the α and f indices. Following the treatment of Chhabra and Jensen [13], which avoids the numerical use of the Legendre transform, we have [14–18]

$$\alpha(q) = \lim_{\varepsilon \to 0} \frac{\sum_{i=1}^{N(\varepsilon)} \hat{p}_i(\varepsilon) \log p_i(\varepsilon)}{\log \varepsilon} \tag{15}$$

$$f(q) = \lim_{\varepsilon \to 0} \frac{\sum_{i=1}^{N(\varepsilon)} \hat{p}_i(\varepsilon) \log \hat{p}_i(\varepsilon)}{\log \varepsilon} \tag{16}$$

where $\hat{p}_i(\varepsilon) = p_i^q(\varepsilon) / \sum_{j=1}^{N(\varepsilon)} p_j^q(\varepsilon)$.

Note that, as expected, expressions (14)–(16) bear a close similarity with those used for the exactly soluble example 1. The second column of table 4 summarizes the computed values of the more relevant multifractal indices in the q-representation for the exactly soluble multifractal of equal size (example 1). The computed results and the exact values show a good agreement only for $q \geqslant 0$ (given their error bars). For very large values of q some round-off errors can be detected. On the other hand, for $q < 0$ the computed $\alpha(q)$ values are significatively greater than the exact ones and this is due to the computational strategy of the implemented algorithm [18].

5.2. Box-counting fixed-mass algorithm

In the case of the box-counting fixed-mass algorithm introduced by Badii and Politi [5, 6] it is shown that from (5),

$$1 - q(\tau) = \lim_{p \to 0} \frac{\log \left[\frac{1}{N(p)} \sum_{i=1}^{N(p)} \varepsilon_i^{-\tau}(p) \right]}{\log p} \tag{17}$$

where $N(p)$ is the number of boxes with measure p used to evaluate the average in (5). Note that $N(p)$, in this case, does not necessarily count all the boxes with equal measure needed to cover the pattern, but only a predefined subset [12, 18]. In this case q is expressed as a function of τ, thus it seems natural to use the τ-representation in order to obtain expressions for $\tilde{\alpha}$ and $\tilde{f}$ indices. With some algebra, and following a similar procedure to that employed for the fixed-size algorithm, we obtain:

$$\tilde{\alpha}(\tau) = \lim_{p \to 0} \frac{\frac{1}{N(p)} \sum_{i=1}^{N(p)} \hat{\varepsilon}_i(p) \log \varepsilon_i(p)}{\log p} \tag{18}$$

$$\tilde{f}(\tilde{\alpha}(\tau)) = \lim_{p \to 0} \frac{\frac{1}{N(p)} \sum_{i=1}^{N(p)} \hat{\varepsilon}_i(p) \log \hat{\varepsilon}_i(p)}{\log p} \tag{19}$$

where $\hat{\varepsilon}_i(p) = \varepsilon_i^{-\tau} / [1/N(p) \sum_{j=1}^{N(p)} \varepsilon_j^{-\tau}]$.

These expressions, again as expected, show close similarities with those used for the exactly soluble example 2, but with the difference that here we take an average over a subset of boxes having the same mass (p).

The last expressions (17)–(19) enable us to implement the fixed-mass box-counting algorithm, and obtain all the multifractal indices directly, i.e. the $\tilde{f}(\tilde{\alpha})$ and then the $f(\alpha)$ spectrum of singularities. These expressions are particularly useful in the study of the multifractal behaviour at $q \leqslant 0$, i.e. at $\tau \leqslant 0$, precisely where the fixed-size algorithm fails. The regression range of p is standardized choosing the maximum value of p of the

distribution as the lowest bound and the maximum value of p resulting from box-counting as the greatest bound [18].

The second column of table 5 summarizes the computed values of some multifractal indices in the τ-representation for the exactly soluble multifractal of equal measure (example 2). The agreement is very good for $q(\tau)$ and for $\tilde{\alpha}(\tau)$ indices, specially for $\tau \ll 0$ ($q \ll 0$) giving a good estimation for $\tilde{\alpha}_{-\infty}$ ($1/\alpha_{-\infty}$), the asymptotic value. However, the $f(\tau)$ index is overestimated, especially for $\tau \ll 0$. This is nothing but an artefact of the computational strategy of the implemented fixed-mass algorithm [18], here applied to an iterated multifractal with few iterations. Actually, we have taken a grid of 512×512 pixels to reproduce the usual working conditions with experimentally determined measures. Then, acceptable standard errors in $\tilde{\alpha}(\tau)$ and $q(\tau)$ indices ($\sim$1%) for $\tau \ll 0$ (e.g. -50) propagate an standard error of 50–100% [18].

5.3. The use of both box-counting algorithms

For the exactly soluble multifractal of different size and different measure (example 3, see figure 3), table 6 summarizes some computed values of multifractal indices in the q-representation obtained using the fixed-size algortihm and table 7 the corresponding results in the τ-representation using the fixed-mass algorithm. For this case, the computed values show good agreement with the exact ones.

Summarizing the above results, we conclude that the fixed-size algorithm should be used in the q-representation and is especially suited for $q \geqslant 0$, whereas the fixed-mass algorithm should be used, complementarily, in the τ-representation where it is especially suited for $\tau \leqslant 0$. Transforming, according to the previously introduced equivalences, we complete either one of the pair of representations to finally end up with a whole range robust and

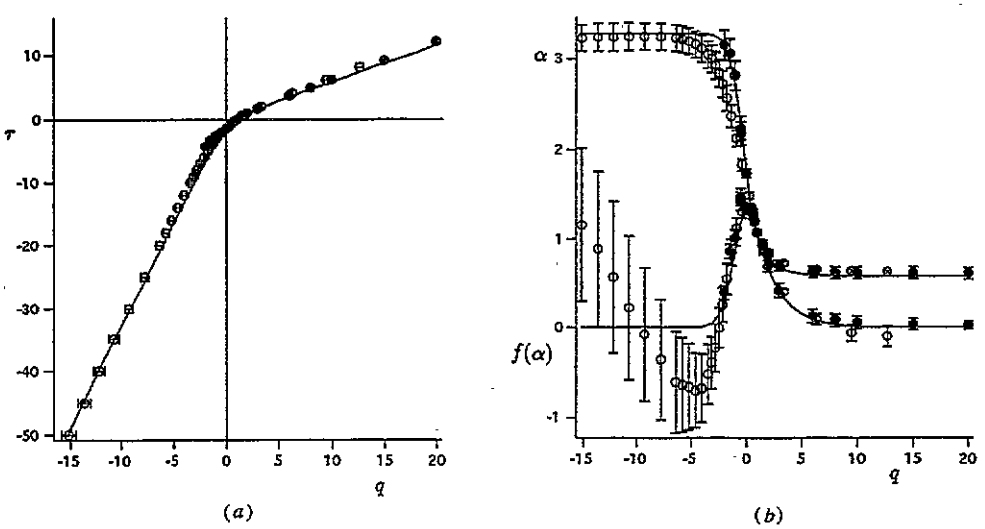

Figure 4. Indices τ versus q (a) and α and $f(\alpha)$ versus q (b) for the exactly soluble example with different size and different measure. The full curve represents the exact behaviour and the discrete points stand for the values computed with the two proposed algorithms: fixed size (●) and fixed mass (○). The regression range for the fixed-size algorithm is $3.43 \leqslant \ell \leqslant 109.7$ pixels. The regression range for the fixed-mass algorithm is the standard. Standard errors on q values, when fixed-mass algorithm is used, are omitted for the sake of simplicity in (b).

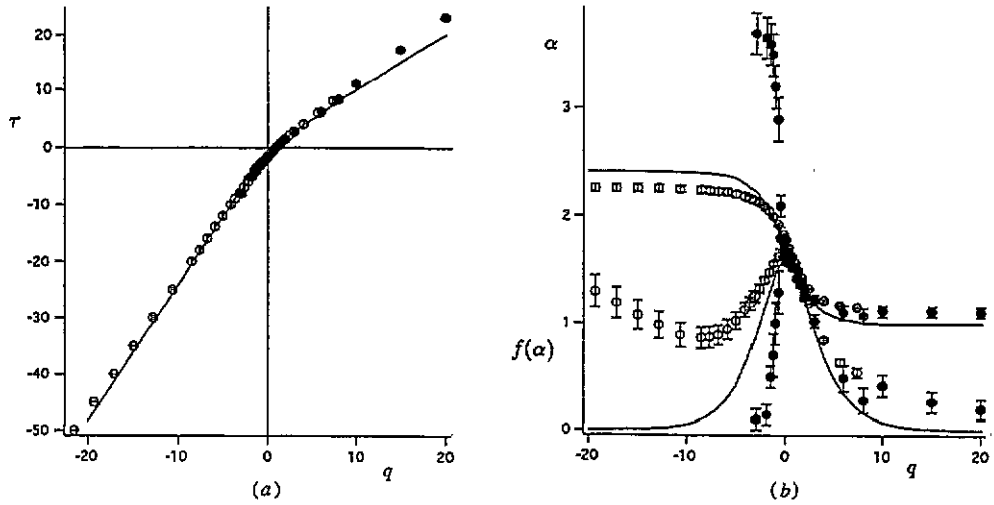

Figure 5. (*a*) Indices τ versus q and (*b*) α and $f(\alpha)$ versus q for the exactly soluble example with equal size and different measure. The full curve represents the exact behaviour and the discrete points stand for the values computed with the two proposed algorithms: fixed size (●) and fixed mass (○). The regression range for the fixed-size algorithm is $2.53 \leqslant \ell \leqslant 47.18$ pixels. The regression range for the fixed-mass algorithm is the standard. Standard errors on q values, when fixed-mass algorithm is used, are omitted for the sake of simplicity in (*b*).

reliable multifractal description [14, 18]. This is exactly the strategy that we have followed to construct the results depicted in figure 4.

To emphasize the appropriateness of the fixed-mass algorithm when trying to evaluate the asymptotic value of $\tilde{\alpha}_{-\infty}$ $(1/\alpha_{-\infty})$, we show in figure 5(*b*) plots of α, $f(\alpha)$ versus q. This figure shows that the estimation of α with the fixed-size algorithm is, for q slightly negative, already almost two times greater than the exact value. In contrast, the α values obtained with the fixed-mass algorithm are very close to the exact ones.

6. Application to experimental measures

Quasi-two-dimensional electrochemical deposition (ECD) is a typical example of pattern formation under non-equilibrium conditions. Typically in these experiments, a metallic deposit is formed in a thin layer of an aqueous electrolyte solution containing the metal cation. It has been clearly shown that different electrodeposit morphologies are obtained when control parameters, including applied potential or current, cation concentration, cell dimensions, etc [19, 20] are adequately modified.

Among the different electrodeposit morphologies, open-fractal structures are formed in zinc electrodeposition experiments using a film cell at small applied potential values (experimental conditions are listed in the caption of figure 6). In this case, fractal concepts are necessary, not only to characterize these aggregates morphologically, but most interestingly to capture the subtle details of their dynamical evolution and general behaviour.

In order to describe the multifractal behaviour of the mass distribution of the open-fractal electrodeposits, a particular electrodeposit is chosen (figure 6) [16, 19, 20]. Figure 7 shows the joined τ versus q function in the q-representation obtained using the fixed-size algorithm for $q \geqslant 0$ and the fixed-mass one for $\tau \leqslant 0$. This linear behaviour corroborates the uniform, non-multifractal, characteristic of the mass distribution measure for a range of

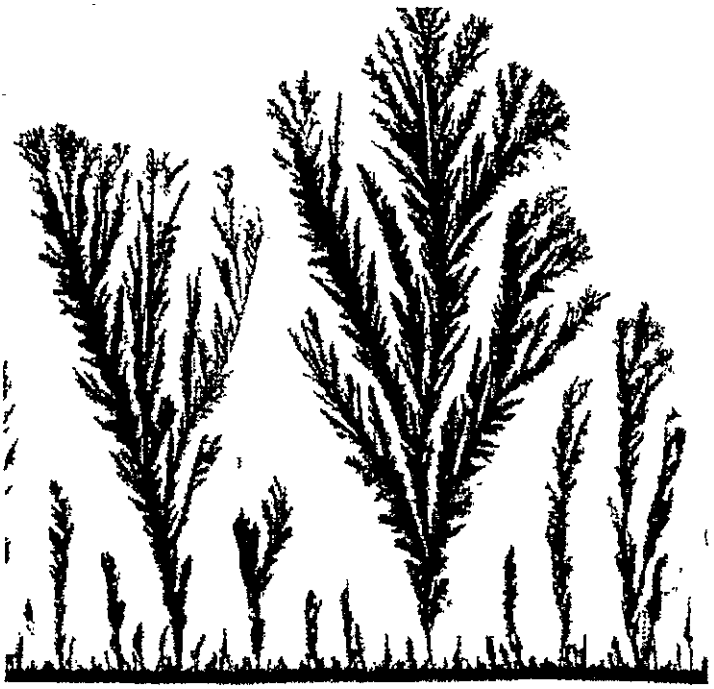

Figure 6. Quasi-two-dimensional electrodeposit grown in a parallel cell (70 μm thickness, electrode length 3.5 cm and electrode separation 3 cm). Open-fractal morphology (512 pixels $\equiv$ 6.5 mm), grown at $[ZnSO_4] = 0.4$ M and $\Delta V = 6$ V.

q ($-28 \leqslant q \leqslant 25$) wider than in any previous work [14, 16, 19, 21]. A linear regression fit of τ versus q gives from its slope the fractal dimension D_f estimated as $\langle D_q \rangle = 1.68 \pm 0.02$, which is in agreement with previous results [14, 16, 19, 21] and similar to that obtained for DLA patterns $D_{f(\mathrm{DLA})} = 1.6$–$1.7$ [14, 22].

In order to gain a better understanding of the growth dynamics governing fractal electrodeposition, we would need to compare the multifractal scaling of the experimentally computed growth probability distribution (GPD), with that corresponding to a Laplacian growth mode [16, 17]. Here, we only present the multifractal scaling behaviour of this measure obtained assuming a Laplacian growth mode [15, 17], for the open-fractal zinc electrodeposit examined above (figure 6). The GPD on every perimeter site of the metallic aggregate is computed here in terms of the normal gradient of a Laplacian field, $\nabla^2 \phi = 0$, solved with boundary conditions $\phi = 0$ at the perimeter and $\phi = 1$ far away from it. In figure 8 plots of τ versus q and α versus q using the fixed-size algorithm for $q \geqslant 0$ and the fixed-mass one for $\tau \leqslant 0$ are shown. A typical multifractal behaviour is obtained. Table 8 summarizes the computed values of some multifractal indices in the q-representation for the GPD measure of this particular open-fractal electrodeposit. Also added are some representative values of the multifractal scaling behaviour of the GPD (harmonic measure) for a typical DLA pattern [23]. Characteristic values for a harmonic measure in simulated DLA patterns are: $D_0 = D_f = 1.6$–1.7 [14, 22], $D_1 = 1$ [24] and $\tau_3 \simeq 1 + \alpha_\infty \simeq D_f$ [25–27]. The somewhat lower computed value of D_0 is due to the contour-regularization effect needed to ensure the convergence of the Laplacian solution [15, 17]. Table 9 summarizes the values obtained for some multifractal indices in the τ-representation for the GPD measure

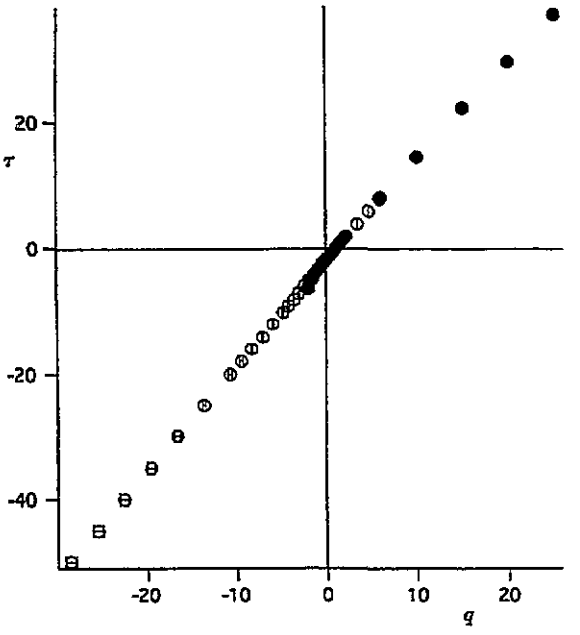

Figure 7. Indices τ versus q for the open-fractal morphology when the mass-distribution measure is analysed. The two algorithms are used: fixed size (●) and fixed mass (○). The regression range for the fixed-size algorithm is 68 μm $\leqslant \ell \leqslant$ 1104 μm. The regression range for the fixed-mass algorithm is the standard.

Table 8. Some representative multifractal indices in the q-representation for the open-fractal morphology when the GPD measure is assumed Laplacian and for a DLA pattern [23]. The regressions in the box-counting fixed-size algorithm applied to the GPD of open-fractal (ECD) are achieved in the range 60 μm $\leqslant \ell \leqslant$ 1100 μm.

q	Singularity exponent	DLA (harmonic measure)	Open fractal (ECD) Laplacian GPD
inf	q	-5	-3
	τ_{inf}	~ -48.0	-7.5 ± 0.8
	α_{inf}	~ 9.0	6.7 ± 0.2
	$f(\alpha_{inf})$	~ 0.0	0.10 ± 0.01
	D_{inf}	~ 7.0	1.9 ± 0.2
0	$f(\alpha_0) = D_f$	1.64 ± 0.1	1.53 ± 0.01
	α_0	~ 4.0	3.41 ± 0.09
1	$D_1 = f(\alpha_1) = \alpha_1$	1.04 ± 0.01	0.983 ± 0.005
3	τ_3	—	1.51 ± 0.02
sup	q	10	15
	τ_{sup}	~ 6	8.8 ± 0.2
	α_{sup}	0.64–0.70	0.61 ± 0.01
	$f(\alpha_{sup})$	~ 0.0	0.069 ± 0.008
	D_{sup}	~ 0.65	0.63 ± 0.01

of this particular open-fractal electrodeposit.

Results for the more active growth sites determined experimentally from the normal velocity of the perimeter growing sites show a robust multifractal behaviour ($q \geqslant 0$) which,

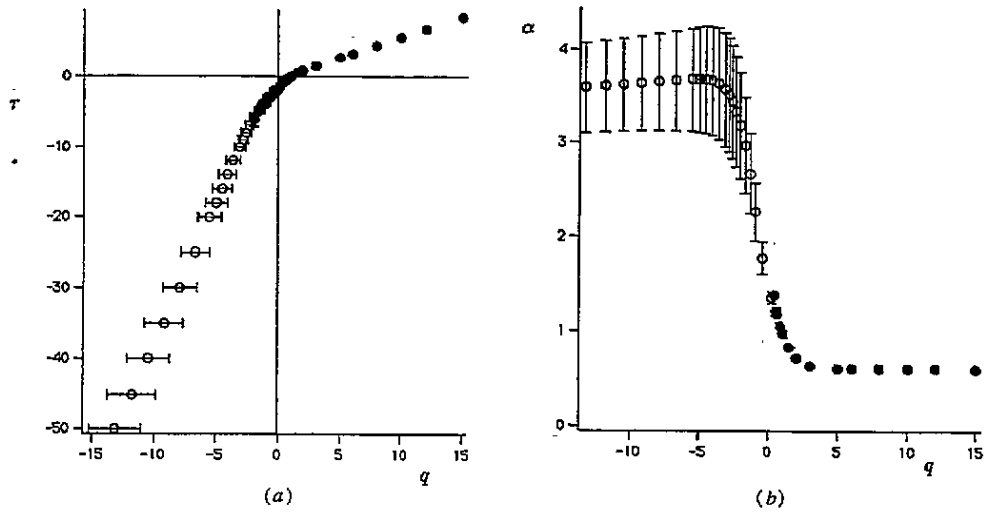

Figure 8. (*a*) Indices τ versus q and (*b*) α versus q for the open-fractal morphology when the GPD measure is assumed Laplacian. The two algorithms are used: fixed-size (●) and fixed-mass (○). The regression range for the fixed-size algorithm is 68 μm $\leqslant \ell \leqslant$ 1104 μm. The regression range for the fixed-mass algorithm is the standard. Standard errors on q values, when fixed-mass algorithm is used, are omitted for the sake of simplicity in (*b*).

Table 9. Some representative multifractal indices in the τ-representation for the open-fractal morphology when the GPD measure is assumed Laplacian. The regression range is the standard in our fixed-mass algorithm.

τ	Singularity exponent	Open fractal Laplacian GPD
inf	τ	-50
	q_{inf}	-13 ± 2
	$\tilde{\alpha}_{inf}$	0.28 ± 0.04
	$\tilde{f}(\tilde{\alpha}_{inf})$	-0.3 ± 0.3
	$\tilde{D}_{inf}$	3.5 ± 0.5
$-D_f$	D_f	1.53 ± 0.01
	q_{-D_f}	-0.19 ± 0.05
	$\tilde{\alpha}_{-D_f}$	0.64 ± 0.04
	$\tilde{f}(\tilde{\alpha}_{-D_f})$	-0.21 ± 0.04
0	$\tilde{D}_0 = 1/\tilde{\alpha}_0$	0.92 ± 0.03
sup	τ	8
	q_{sup}	11.2 ± 0.5
	$\tilde{\alpha}_{sup}$	1.33 ± 0.07
	$\tilde{f}(\tilde{\alpha}_{sup})$	-0.5 ± 0.1
	$\tilde{D}_{sup}$	0.79 ± 0.04

within the length scale range examined is compatible with a Laplacian growth mode [16, 17]. Further work is in progress in order to extend this experimental comparison at $\tau \leqslant 0$ using the fixed-mass algorithm [18].

7. Concluding remarks

A new formalism, based on the τ-representation, allows us to introduce the box-counting fixed-mass algorithm in a natural way. This procedure is especially suited for $\tau \leqslant 0$ ($q \leqslant 0$) when estimating $q(\tau)$ and $\tilde{\alpha}(\tau)$. The box-counting fixed-mass algorithm complements, in this way, the box-counting fixed-size algorithm, which is appropriate for the estimation of the multifractal indices in the range of $q \geqslant 0$ ($\tau \geqslant 0$).

Another important success of the fixed-mass algorithm is the accuracy attained in evaluating the asymptotic value of $\tilde{\alpha} = \tilde{\alpha}_{-\infty}$ ($1/\alpha_{-\infty}$), in contrast with that obtained when the fixed-size algorithm is used.

The simultaneous application of these two algorithms allows us to extend the range of q to study the multifractal behaviour of some distributed measure, obtained either mathematically or experimentally.

Acknowledgments

One of us (JM) benefited from FPI grant from Ministerio de Educación y Ciencia (Spain). We are grateful to the 'Centre de Supercomputació de Catalunya (CESCA)' for providing us with computational facilities. Financial support from Dirección General de Investigación Científica y Tecnológica (DGICYT, Spain) under projects PB90-0455 and PB93-0759 are acknowledged. We are also grateful to the interesting comments of Dr R Riedi.

References

[1] Mandelbrot B B 1988 *Fractals and Multifractals: Noise, Turbulence and Galaxies* (New York: Springer)
[2] Vicsek T 1989 *Fractal Growth Phenomena* (Singapore: World Scientific)
[3] Falconer K J 1993 The multifractal spectrum of statistically self-similar measures *Report* PM-93-01, University of Bristol
[4] Cawley R and Mauldin R D 1992 *Adv. Math.* **92** 196
[5] Badii R and Politi A 1984 *Phys. Rev. Lett.* **52** 1661
[6] Badii R and Politi A 1985 *J. Stat. Phys.* **40** 785
[7] Halsey T C, Jensen M H, Kadanoff L P, Procaccia I and Shraiman B I 1986 *Phys. Rev.* A **33** 114
[8] Grassberger P 1983 *Phys. Lett.* **97A** 227
[9] Grassberger P and Procaccia I 1984 *Physica* **13D** 34
[10] Hentschel H G E and Procaccia I 1983 *Physica* **8D** 435
[11] Stanley H E and Meakin P 1988 *Nature* **335** 405
[12] Broggi G 1988 *J. Opt. Soc. Am.* B **5** 1020
[13] Chhabra A and Jensen R V 1989 *Phys. Rev. Lett.* **62** 1327
[14] Argoul F, Arneodo A, Elezgaray J and Grasseau G 1990 *J. Chim. Phys.* **87** 1487
[15] Mas F and Sagués F 1992 *Europhys. Lett.* **17** 541
[16] Trigueros P P, Mach J, Claret J, Mas F and Sagués F 1993 *Fractals* **1** 439
[17] Mach J, Mas F and Sagués F 1994 *Europhys. Lett.* **25** 271
[18] Mach J 1995 *PhD Thesis* Universitat de Barcelona, Barcelona, Spain
[19] Trigueros P P, Claret J, Mas F and Sagués F 1991 *J. Electroanal. Chem.* **312** 219
[20] Trigueros P P, Claret J, Mas F and Sagués F 1992 *J. Electroanal. Chem.* **328** 165
[21] Sagués F, Mas F, Vilarrasa M and Costa J M 1990 *J. Electroanal. Chem.* **278** 351
[22] Meakin P 1989 *The Fractal Approach to Heterogeneous Chemistry: Surfaces, Colloids and Polymers* ed D Avnir (New York: Wiley)
[23] Hayakawa Y, Sato S and Matsushita M 1987 *Phys. Rev.* A **36** 1963
[24] Makarov N G 1985 *Proc. London Math. Soc.* **51** 369
[25] Turkevich L and Scher H 1985 *Phys. Rev. Lett.* **55** 1026
[26] Halsey T C, Meakin P and Procaccia I 1986 *Phys. Rev. Lett.* **56** 854
[27] Halsey T C 1987 *Phys. Rev. Lett.* **59** 2067